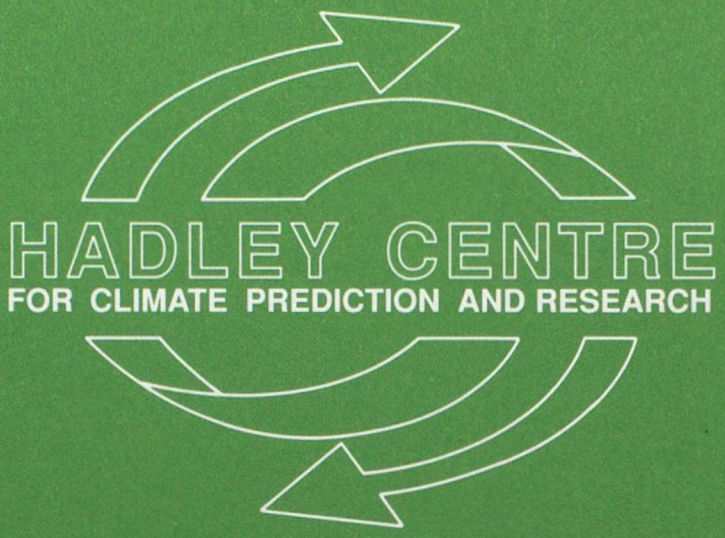

A simulation of seasonality in ENSO forecast skill

by

M. K. Davey, D. L. T. Anderson, S. Lawrence

CRTN 38

May 1993

CLIMATE
RESEARCH
TECHNICAL
NOTE

Hadley Centre
Meteorological Office
London Road
Bracknell
Berkshire RG12 2SY

CLIMATE RESEARCH TECHNICAL NOTE NO. 38

A SIMULATION OF SEASONALITY IN ENSO FORECAST SKILL

by

M.K. Davey, D.L.T. Anderson, S. Lawrence

Hadley Centre for Climate Research and Prediction
Meteorological Office
London Road
Bracknell
Berkshire RG12 2SY
U.K.

Note: This paper has not been published. Permission to quote from it should be obtained from the Director of the Hadley Centre

A simulation of seasonality in ENSO forecast skill

M.K. Davey (+), D.L.T. Anderson (*), S. Lawrence (*)

(*) Department of Physics, Clarendon Laboratory, Parks Road, Oxford

(+) Hadley Centre, UK Meteorological Office, London Road, Bracknell

Abstract

The skill of long range forecasts of ENSO events depends on season. In an attempt to find a possible explanation for this dependence, a highly idealised delayed-oscillator model has been used to simulate such forecasts. The model contains seasonally-varying internal parameters to represent a seasonally-dependent basic state. Although the skill of the artificial forecasts shows substantial dependence on both seasonal and ENSO phase, we find that the seasonal variation in our model is due to seasonal phase- locking of the ENSO cycle, and does not depend directly on changes in basic state. It is suggested that the seasonal skill changes found in practice may be at least partly due to the same effect.

1. Introduction

For the past few years dynamical forecasts of the El Niño Southern Oscillation (ENSO) cycle in the tropical Pacific region have routinely been made using a coupled ocean-atmosphere model (Cane et al. 1986, Zebiak & Cane 1987). These forecasts typically have useful predictive skill for lead times of up to a year. The skill is seasonally variable with a marked decrease of skill commonly occurring in northern spring (see Fig. 1). Such variation has also been found in predictability experiments by Goswami & Shukla (1991) using the Cane & Zebiak model. Similar seasonal variations have been noted in other ENSO forecast models (Barnston & Ropelewski 1992, Latif & Flügel 1991, Latif & Graham 1991, Graham et al. 1987), and discussed in the review by Latif

et al. (1993). One possible cause of this variation in skill is that changes in the stability of the state of the forecast model lead to different error growth conditions. In this note we use a highly-idealised model to explore this possibility.

Various forms of the delayed-oscillator equation have been used to help explain the oscillatory behaviour of more complex ENSO models, including the Cane & Zebiak model as analysed by Battisti (1988). (See the review by McCreary & Anderson 1991.) We consider here the simple form originally proposed by Schopf & Suarez (1988), wherein the delayed oscillator is an ordinary differential equation for sea surface temperature (SST) anomalies in a region of strong ocean-atmosphere interaction, with the delay term accounting for the remote-forcing effect of equatorially-trapped ocean waves that travel away from the interaction region and then return via reflection from coasts. The novel aspect here is that parameters in this equation are allowed to vary seasonallly.

The behaviour for several parameter choices will be considered. In each case a control integration is made, followed by a series of 'forecasts'. Each forecast is initialised using control values plus random perturbations, then integrated forward for a few seasons. Standard skill assessments are made. We find that skill usually varies markedly through both the ENSO cycle and the seasonal cycles.

2. Equations

In dimensional form, the delayed oscillator equation for the temperature perturbation T^* in the interaction region can be expressed as

$$T^*_{t^*} = k\{T^*[1-(T^*/T_0)^2] - \alpha T^*(t^*-d)\} \tag{1}$$

where k is a growth rate representing air-sea interaction, T_0 is a measure of the limit to SST growth due to nonlinear effects, α is a non-dimensional measure of the efficiency of reflected waves, and d measures the time delay induced by wave propagation and reflection.

The parameters d and α are allowed to vary seasonally, according to

$$d = d_0 + d_1 \sin(2\pi t^*/\tau^*) \tag{2}$$

$$\alpha = \alpha_0 + \alpha_1 \sin(2\pi t^*/\tau^*) \tag{3}$$

where τ^* is equal to one year. Such changes in α and Δ could arise in practice through e.g. seasonal changes in equatorial current patterns and amplitudes. Note that no

attempt is made here to identify the phase of the model seasonal variations with actual seasons. Seasonal dependence could also be introduced via the growth rate k or by specifying some external forcing term: the latter has been partly explored by Wu et al. (1993).

Non-dimensional variables are defined by

$$T = T^*/T_0 \qquad t = t^*k \qquad \tau = \tau^*k$$

$$\Delta_0 = d_0 k \qquad \Delta_1 = d_1 k$$

so (1) becomes

$$T_t = T - T^3 - \alpha T(t-\Delta) \tag{4}$$

where

$$\Delta = \Delta_0 + \Delta_1 \sin(2\pi t/\tau)$$

Thus the non-dimensional parameters are α_0, α_1, Δ_0, Δ_1, and τ. Note that choosing a value for τ is equivalent to choosing the dimensional coupling coefficient k, because $k = \tau/\tau^*$.

Solutions of equ. (4) with no seasonal cycle ($\alpha_1 = \Delta_1 = 0$) are described in McCreary & Anderson (1991), and can be divided into stable and oscillatory parameter regimes in (α_0, Δ_0) space, separated by a critical curve, as shown in Fig. 2. From a linear stability analysis, the equation for the critical curve is

$$\Delta = \arccos(\beta/\alpha) \;/\; \sqrt{\alpha^2 - \beta^2} \tag{5}$$

where

$$\beta = 1 \qquad \text{if } \alpha > 1$$
$$\beta = 3\alpha - 2 \qquad \text{if } \alpha < 1$$

Above the critical curve all solutions oscillate; below the curve there are steady solutions, co-existing with oscillations in some small regions (see McCreary & Anderson 1991). The oscillatory solutions have some intrinsic nondimensional 'ENSO' period, E_0 say: this period is equivalent to E_0/τ seasonal cycles when a value for τ is chosen.

When parameters are allowed to vary seasonally then the oscillatory solutions for parameters close to the critical curve tend to phase-lock to the seasonal cycle with a modified period E, while for parameters further from the critical curve (the distance depending on the amplitude of the seasonal variations of α_0 and Δ_0) the seasonal effect

is negligible or confined to weak modulation of the intrinsic oscillation with period E_0. Phase-locking could occur when Δ and/or α varied seasonally.

Parameters for six phase-locked cases with varying α or Δ are listed in Table 1, and their positions in α, Δ space are indicated in Fig. 2. In cases I, II and IV the seasonal variation of the parameters moved the system to and fro across the critical curve in (α_0, Δ_0) space, while the other cases always remained in the purely oscillatory region.

3. Forecast method for regular oscillations

Equ. (4) was integrated using a timestep δt set to the equivalent of 6 days (giving 60 steps per seasonal cycle), and the temperatures T were saved once regular oscillations had been established. These temperatures were also used to provide spot-value control 'observations' C_i at monthly intervals, for N ENSO cycles of K years each, giving a total of $12NK$ values, where K is an integer. For convenience, results will be discussed in terms of years and months, with a 360-day year. Forecasts F_{ij} were made of each C_i as described below, with a lead time of j months ranging from $j = 1$ to $j = 36$.

A forecast made from a time t_0 (say) was initialised by setting T to the saved control values in the 'memory' period $t_0 - \Delta$ to t_0, and then adding a random perturbation to the last two values at t_0 and $t_0 - \delta t$. These perturbations were drawn uniformly from the range (-0.5,0.5). The same perturbations were used throughout one ENSO cycle, then a new choice made for the next ENSO cycle. (Here, with each ENSO cycle identical, the process is equivalent to using N sets of initial perturbations for forecasts for one ENSO cycle. Typically $N = 25$ was large enough for statistical quantities to stabilise: some cases were checked using $N = 100$.) Fig. 3 shows the evolution of some sample forecasts from case I, with each forecast starting at the same ENSO phase with the same 'memory', but with different random initial perturbations. The 'memory' component means that most tend to follow the same general trajectory at first: in Fig. 3a all but 3 of the 25 trajectories move initially into a cold phase. Note that each forecast will eventually itself settle into a regular oscillation, but not necessarily with the same phase as the control cycle. In case I the ENSO period is 4 years, phase locked to the seasonal cycle, so there are 4 possible interannual phases for the regular oscillation. Fig. 3b shows that after some time the sample forecasts have in this case settled onto 3 of the 4 possibilities. (With a wider sample of initial conditions all 4 possibilities would be realised.)

The forecasts were then analysed by taking averages with the ENSO or seasonal phase fixed. It is convenient to label values by writing

$$i = [(n-1)K + k - 1]12 + m \qquad (6)$$

for month m of year k of cycle n ($m = 1...12$, $k = 1...K$, $n = 1...N$). We further put

$$i = 12K(n-1) + l$$

where

$$l = 12(k-1) + m \qquad (7)$$

for $l = 1...12K$. Thus m is a label for the month (phase) of the year, and l is a label for the month (phase) of the ENSO cycle. Note that a forecast labelled mj (or lj) actually starts in month-of-year $(m-j)$mod 12 (or starts in month-of-ENSO $(l-j)$mod $12K$).

The various standard statistical quantities referred to below are defined in the appendix. Consistently, $\hat{}$ will indicate an average with the ENSO phase fixed (i.e. l fixed), $<>$ will denote an average with the seasonal phase fixed (i.e. m fixed), and an overbar will denote an average over all i.

4. Forecast statistics for case I

The ENSO cycle average control $\hat{C}_l$ and forecast $\hat{F}_{lj}$ with j=12 months are shown for case I in Fig. 4, along with the standard deviation σ_{lj} of the forecast values and the rms error e_{lj}. There is considerable variation through the cycle in both the standard deviation, that is a measure of the scatter in the forecasts, and the rms error. These two quantities are similar in pattern and amplitude: the difference is related to the generally small 'systematic error' $S_{lj} = \hat{F}_{lj} - \hat{C}_l$ by equ. (A7). The forecasts here are more accurate and more self-consistent around months 24 and 48, i.e. when starting just before troughs (month 14) and peaks (month 38) in this ENSO cycle. The near-symmetry of forecasts for positive ('warm') and negative ('cold') phases of the ENSO cycle is a consequence of the symmetry of the delayed oscillator equation (4). (Forecasts would be exactly symmetric if the initial perturbations were forced to have the opposite sign for 'warm' and 'cold' starts.)

Fig. 5a shows how e_{lj} varies with forecast length j and ENSO phase $(l-j)$mod 48 at the forecast start, for case I. Contours of e_{lj} are largely horizontal in this view, indicating that the error depends on the ENSO phase at the start of the forecast, rather than the ENSO phase at the end of the forecast. Errors tend to be large when starting at or before transition of the ENSO cycle ($(l-j)$mod $48 = 5, 29$), and small when starting at or before extrema ($(l-j)$mod $48 = 14, 38$), as seen in Fig. 4. The largest errors occur when a forecast starts just before transition, and ends near the next extremum. Contours of σ_{lj} (not shown) have a very similar pattern.

It is not surprising that skill varies markedly when starting from considerably different initial ENSO phases. It is perhaps less obvious that skill will depend on the

seasonal cycle, when different ENSO phases are averaged together. Fig. 5b shows how the case I rms error e_{mj}, averaged to the annual cycle, depends on length j of forecast and on start month-of-year $(m-j)$mod 12. (This is essentially an rms average of Fig. 5a along the vertical (constant j) axis, at annual intervals.) All errors tend to grow similarly for the first 8 months, slightly less rapidly around start month 8. Variation with seasonal phase is markedly less than that for ENSO phase. Differences become more noticeable for larger j (longer lead times): contour orientations in Fig. 5b change from vertical toward horizontal on the page as errors depend more on start month than on j. For start months 7 to 10 errors actually decrease substantially as j increases, rising again for $j > 17$. Errors do not depend consistently on the month m for which the forecast is made: see Fig. 6a which shows e_{mj} plotted with m as the vertical axis (this is essentially a vertically sheared version of Fig. 5b).

The correlation r between forecasts and control is also sometimes used as a measure of skill. Fig. 6b shows r_{mj} for case I as a function of start month and forecast length: the pattern is quite similar to Fig. 5b, with high correlation corresponding to low rms error. Dependence on start month for low j is greater in Fig. 6b, with best skill for start month 8.

The secondary maximum in forecast skill around $j = 17$ is reminiscent of the secondary maximum found using more realistic ENSO models (see Goswami & Shukla 1991). Although skill does vary with the seasonal cycle in this artificial model, there is however no prominent 'barrier' (that is, a particular month where forecast skill declines markedly) corresponding to that found for actual forecasts as in Fig. 1.

The result of averaging all forecasts for fixed j can be seen for case I in Fig. 7. After an initial rise the rms error e_j shows little change as j increases, and remains smaller than the standard deviation σ of the control. For comparison the persistence error is also shown:

$$pe_j = \overline{(P_{ij} - C_i)^2} \quad , \tag{8}$$

where the persistence forecast is

$$P_{ij} = C_{i-j,j} \quad . \tag{9}$$

Because the control is a regular cycle, pe_j oscillates with the same frequency. Generally $e_j < pe_j$, so the 'dynamical' model is better than persistence. For the first few months the persistence forecast is better, because it starts with zero error whereas the 'dynamical' initial conditions contain random noise. (This feature also appears in practice for forecasts (e.g. the Cane & Zebiak model) which do not assimilate SST data.)

Note that simple persistence as defined by (9) is a poor estimator for an oscillating system: persistence of an oscillation (even a simple fitted sinusoid) would be a much

better non-dynamical estimator. In practice, this behaviour is reflected in the ability of Principal Oscillation Pattern (POP) models of ENSO (e.g. Xu & von Storch 1990) to perform better than simple persistence.

5. The source of seasonal skill variations

The question arises as to whether and how the skill variation seen in this model might be related to the seasonal cycle in the 'reflection' and delay parameters α and Δ. Case II has the same parameters as case I, but with Δ varying seasonally instead of α (see Table 1): results were very similar to case I, which suggests that details of the internal dynamics are not important.

Case N has the same α_0 and Δ_0 as cases I and II, but no seasonal cycle ($\alpha_1 = \Delta_1 = 0$). The nondimensional oscillation period is $E_0 = 11.24$, so by choosing $\tau = 2.87$ that oscillation period corresponded to 4 years, as in case I. Errors etc. were calculated as for case I, and again very similar results (apart from a phase shift) were obtained for both ENSO and seasonal skill variation, as shown in Fig. 8. Evidently the variation in skill does not depend explicitly on the seasonal cycle of α or Δ! The seasonal skill variation is purely a consequence of the ENSO cycle always peaking at the same time of year, as it does for the case N control.

The forecast trajectories for case I and case N, starting from the same ENSO phase and initial perturbations, are very similar for several months (hence the similarity in skill). They eventually differ: case N has no seasonal phase locking, so the forecasts settle into regular oscillations with arbitrary phase, as can be seen for sample trajectories in Fig. 9. The slow separation of case I and case N forecasts indicates that the seasonal effects in case I are weak and that the timescale for return to regular oscillation is long.

6. Cases III-VI

Cases III and IV are in a region of parameter space (see Fig. 2) where oscillations are weak, with amplitudes of 0.5 . Both cases have the same seasonally-varying α, but slightly different Δ: the difference causes case IV to have a 5-year ENSO cycle, whereas III has a 4-year cycle. Errors e_{lj} and e_{mj} for case IV are given in Fig. 10. Errors show the same general ENSO phase dependence as in case I (largest starting at or before transition etc.), but seasonal dependence is very weak, particularly for case IV with the longer ENSO cycle. The very small variation with start month of e_{mj} in Fig. 10 is probably not significant.

Cases V (varying α) and VI (varying Δ) are in a region of phase space where

parameters are close to those derived by Battisti & Hirst (1989) for the Cane & Zebiak model, and oscillations have amplitude greater than unity. Errors again have ENSO phase dependence similar to case I, but have lower amplitude (see Fig. 11a for case V). The forecasts are more tightly constrained to the control than for case I. The seasonal dependence of e_{mj} (see Fig. 11b) in case V is strong up to lead time $j = 12$ months, and error tends to decrease with increasing j, in contrast to case I (Fig. 6a). Slopes of the contours indicate a seasonal barrier: errors increase (or stop decreasing) when a forecast reaches month $m = 9$ of the seasonal cycle. Conversely, errors tend to decrease when month $m = 2$ is reached.

The seasonal barrier is illustrated in a different way in Fig. 12, which shows the evolution of seasonally averaged correlation coefficients r_{mj} for start months 1,4,7 and 10. The abscissa is $j + (m - j) \bmod 12$, so all curves are aligned to the same month-of-year. The tight constraint to the control in case V means that r is always high, and r usually increases at first. In month-of-year 9 forecasts lose skill to some extent, then recover early in the next year. (The large recovery is partly due to the artificial regularity of our model.) In practice ENSO forecasts tend to lose skill in northern spring, as in Fig. 1. In our simple model months are not intended to correspond to particular calendar months: with suitable adjustment of phase in (2) and (3) the seasonal barrier could be moved to any m.

7. Dependence on initial perturbation

It is likely that the pattern of errors will depend on the size of the initial errors. Case I was repeated, but with initial perturbations drawn uniformly from the range (-0.05,0.05), one-tenth of the range for case I. For the ENSO cycle rms error e_{lj} (Fig. 13a cf Fig. 5) now depends more on the month being forecast for, and less on the start month. The regions of relatively large e_{lj} are narrow, tend to be oriented along lines of constant l, and occur for forecasts for the interval between a transition and the next ENSO extremum.

The narrowness of the e_{lj} peaks and their orientation leads to substantial seasonal variation in e_{mj} (Fig. 13b) particularly for j up to about 16 months. This is in marked contrast to the pattern for large initial perturbations (Fig. 6a). There is a tendency for errors to grow once month m=3 of the seasonal cycle is reached: a 'seasonal barrier'.

8. Irregular oscillations

In practice ENSO is far from regular. The experiments were repeated, with an extra random forcing term R added to the RHS of the delayed oscillator equation (4). At each time step R took random values evenly distributed in the range (-2.5,2.5). A segment of the control series C_i thus obtained for parameters as in case I is shown in Fig. 14. Forecasts made with random forcing included showed no significant seasonal skill variation: e_{mj} for one sample is given in Fig. 15. (The small seasonal variation in Fig. 15 is altered when different sample of the random forcing is applied.)

The result is perhaps not surprising, given that seasonal variation of parameters had very little effect in the previous cases considered, beyond defining a regular ENSO period with an integer number of years. Once random forcing was added, the tendency for ENSO always to peak at the same time of year was lost.

ENSO phase averages based on compositing could also be made, but were not attempted here. Perhaps they should be tried: dependence of skill on extremum versus transition could be significant, and this aspect has not been looked at much yet in practice.

9. Summary

The skill of multi-seasonal forecasts has been investigated using a very simple model with artificial 'ENSO' oscillations. The model included seasonally-varying parameters to simulate seasonal changes in the basic state: the aim was to see how the model skill varied with seasonal and ENSO phase, to help explain the seasonal skill variation found in practice.

The seasonal parameter variation allowed the regular model interannual oscillations to lock on to a period of an integer number of years. The model ENSO then always peaked at the same time of year, and in these conditions skill (as measured by forecast rms error or correlations) did vary substantially with both ENSO and seasonal phase, with a tendency for largest errors to occur when starting a forecast near a transition (i.e. starting when ENSO amplitude was near zero, passing between 'warm' to 'cold' or vice versa). There was also some evidence of a 'seasonal barrier', with errors growing more strongly at certain times of year.

This behaviour did not depend intrinsically on the seasonal parameter changes, however: very similar results were obtained with constant parameters by simply tuning the timescale to give an ENSO period with an integer number of years. The skill variation thus depended on the tendency for ENSO always to peak at the same time of

year, regardless of the cause. When random forcing is added to the simple model, the tendency for ENSO to always peak at the same time of year is lost, and seasonal skill dependence is also lost.

Thus the main result of our investigation is that seasonal variations in forecast skill are not necessarily primarily due to changes in the basic state of the system. The phase of the ENSO cycle itself dominates the skill variation in our model: seasonal variation is determined by seasonal phase locking of the ENSO cycle, which may be due to a number of causes. Further investigations to determine how skill varies with ENSO phase in practice are recommended.

Appendix A: Definitions of some statistical quantities

Suppose the ENSO cycle is regular with a period of K years, and forecast and control values are saved monthly for N ENSO cycles. Indices i, l, m are as defined in section 3. An average of some quantity a with ENSO phase index l fixed is denoted

$$\hat{a}_l = \frac{1}{N}\sum_{n=1}^{N} a_i \quad , \tag{A1}$$

an average for fixed seasonal phase m is denoted

$$< a >_m = \frac{1}{KN}\sum_{n=1}^{N}\sum_{k=1}^{K} a_i \quad , \tag{A2}$$

and an average over all values is denoted

$$\overline{a} = \frac{1}{12KN}\sum_{n=1}^{N}\sum_{k=1}^{K}\sum_{m=1}^{12} a_i \quad . \tag{A3}$$

The rms forecast error e_{lj} for the ENSO cycle is defined by

$$e_{lj}^2 = \widehat{(F_{ij} - C_i)^2} \quad , \tag{A4}$$

and the standard deviation is

$$\sigma_{lj} = \widehat{F^2}_{lj} - (\hat{F}_{lj})^2 \quad . \tag{A5}$$

The systematic error for the ENSO cycle is defined as

$$S_{lj} = \hat{F}_{lj} - \hat{C}_l \tag{A6}$$

Note that because the ENSO cycles are identical for the control, $\hat{C}_l = C_i$ and $\widehat{C^2}_l = C_i^2$. Thus the control standard deviation vanishes: $\sigma_l = \widehat{C^2}_l - (\hat{C}_l)^2 = 0$. Further,

$$e_{lj}^2 = \sigma_{lj}^2 + S_{lj}^2 \quad . \tag{A7}$$

Similarly, for the seasonal cycle rms error is defined by

$$e_{mj}^2 = < (F_{ij} - C_i)^2 > = \frac{1}{K}\sum_{k=1}^{K}(e_{lj})^2 \quad , \tag{A8}$$

standard deviations are

$$\sigma_{mj} = < F^2 >_{mj} - < F >_{mj}^2 \quad , \tag{A9}$$

$$\sigma_m = < C^2 >_m - < C >_m^2 \quad , \tag{A10}$$

systematic error is

$$S_{mj} = < F >_{mj} - < C >_m \quad , \tag{A11}$$

and the correlation coefficient for forecasts and control is

$$r_{mj} = \frac{< CF >_{mj} - < C >_m < F >_{mj}}{\sigma_m \, \sigma_{mj}} \quad . \tag{A12}$$

These quantities are related by

$$e_{mj}^2 = \sigma_{mj}^2 + S_{mj}^2 - 2 r_{mj} \sigma_{mj} \sigma_m \quad . \tag{A13}$$

Similar quantities e_j, σ_j, σ, r_j and S_j for averages over all values for a particular lag j are obtained by dropping the subscript m and replacing <> by overbar in (A8) to (A13).

The definitions and relations for seasonal and all-value averages are also valid when the ENSO cycle is not regular.

References

Barnston AG, Ropelewski CF (1992) Prediction of ENSO episodes using canonical correlation analysis. J Clim 5:1316-1345

Battisti DS (1988) The dynamics and thermodynamics of a warming event in a coupled tropical atmosphere/ocean model. J Atmos Sci 45:2889-2919

Battisti DS, Hirst AC (1989) Interannual variability in a tropical atmosphere-ocean model: influence of the basic state, ocean geometry and nonlinearity. J Atmos Sci 46:1687-1712

Cane MA, Zebiak SE (1985) A theory for El Niño and the Southern Oscillation. Science 228:1085-1087

Cane MA, Zebiak SE, Dolan SC (1986) Experimental forecasts of El Niño. Nature 321:827-832

Goswami BN, Shukla J (1991) Predictability of a coupled ocean-atmosphere model. J Clim 4:3-22

Graham NE, Michaelsen J, Barnett TP (1987) An investigation of the El Niño-Southern Oscillation cycle with statistical models. 2. Model results. J Geophys Res 92:14271-14289

Latif M, Flügel M (1991) An investigation of short range climate predictability in the tropical Pacific. J Geophys Res 96:2661-2673

Latif M, Graham NE (1991) How much predictive skill is contained in the thermal structure of an oceanic GCM? J Phys Oceanog 22:951-961

Latif M, Barnett TP, Cane MA, Flügel M, Graham NE, von Storch H, Xu J-S, Zebiak SE (1993) A review of ENSO prediction studies. J Clim in press.

McCreary JP, Anderson DLT (1991) An overview of coupled ocean-atmosphere models of El Niño and the Southern Oscillation. J Geophys Res 96:3125-3150

Schopf PS, Suarez MJ (1988) Vacillations in a coupled ocean-atmosphere model. J Atmos Sci 45:549-566

Wu D-H, Anderson DLT, Davey MK (1993) External impacts on ENSO. J Clim to appear.

Xu J-S, von Storch H (1990) Predicting the state of the Southern Oscillation using principal oscillation patterns. J Clim 3:1316-1329

Zebiak SE, Cane MA (1987) A model El Niño-Southern Oscillation Mon Weath Rev 115:2262-2278

Table 1: Parameters for selected cases for which the period E/τ years is an integer

case	α_0	α_1	Δ_0	Δ_1	τ	E/τ
N	0.7	0.0	2.0	0.0	2.87	4
I	0.7	0.1	2.0	0.0	3	4
II	0.7	0.0	2.0	0.2	3	4
III	1.0	0.1	1.2	0.0	2	4
IV	1.0	0.1	1.1	0.0	2	5
V	1.8	0.2	1.2	0.0	1	4
VI	1.8	0.0	1.2	0.2	1	4

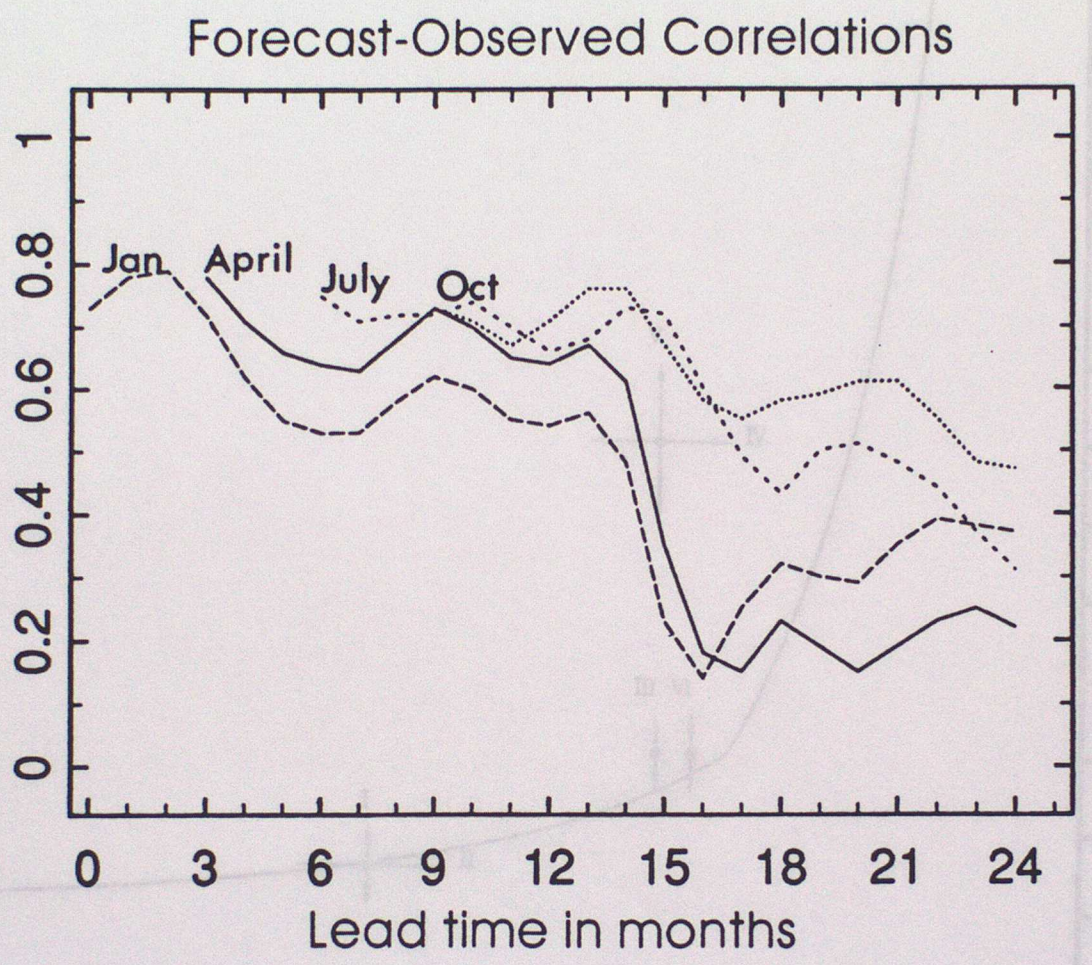

Fig. 1: Correlations of SST anomaly forecasts from the Cane & Zebiak model with observations in the Nino3 region. The forecasts start in the months indicated by each curve. The correlations tend to decrease sharply as forecasts pass the spring season (month 15). (Taken from the CLIVAR brochure, WCRP Sept. 1992.)

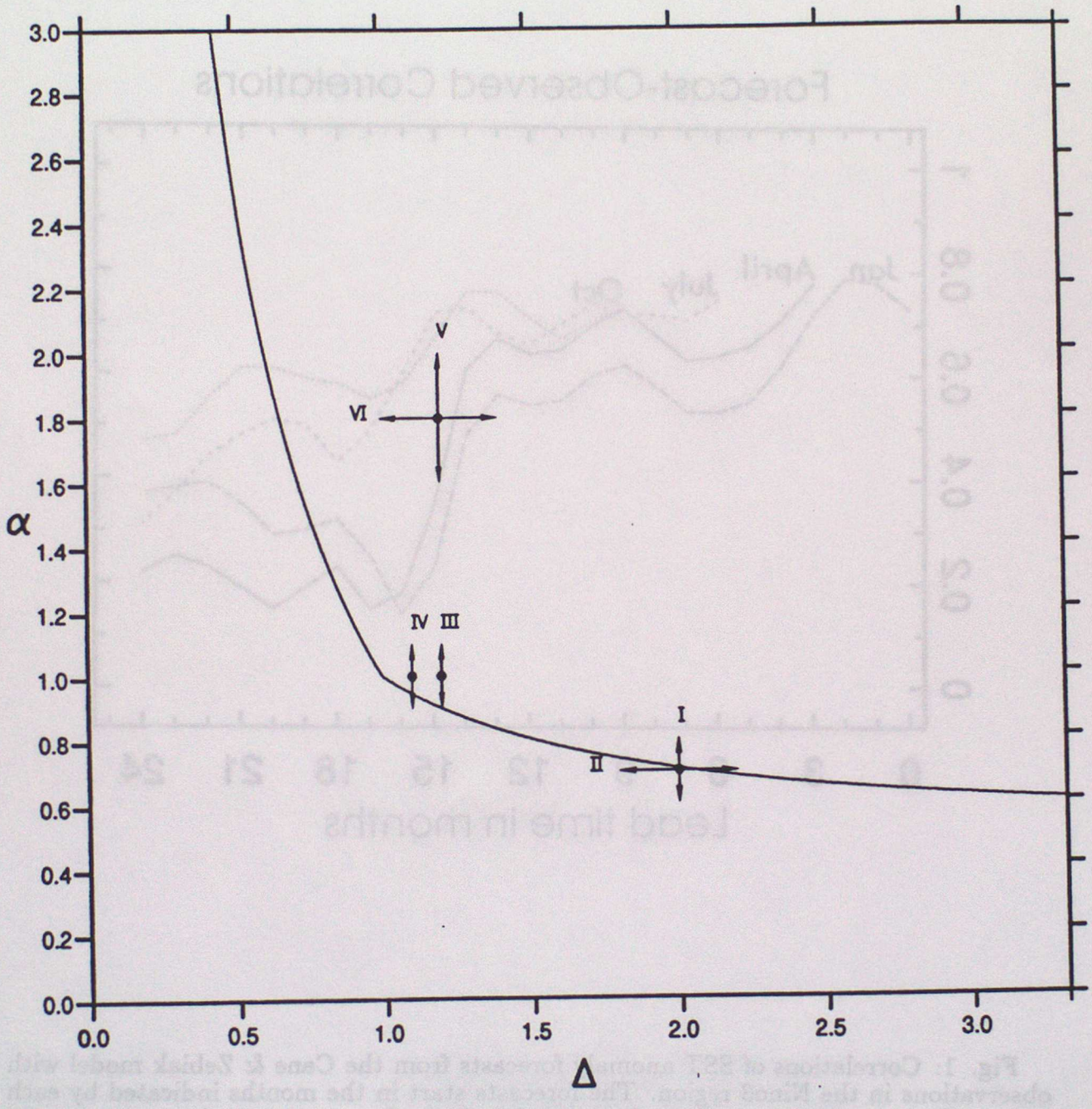

Fig. 2: The behaviour of the delayed oscillator depends on the parameters α and Δ. In the absence of a seasonal cycle ($\alpha_1 = \Delta_1 = 0$) the delayed oscillator equation (4) has steady solutions in the region below the critical curve, and only oscillatory solutions above the curve. Parameters for the particular cases I to VI described in the text are indicated, showing the range of the seasonal cycle in α or Δ in each case.

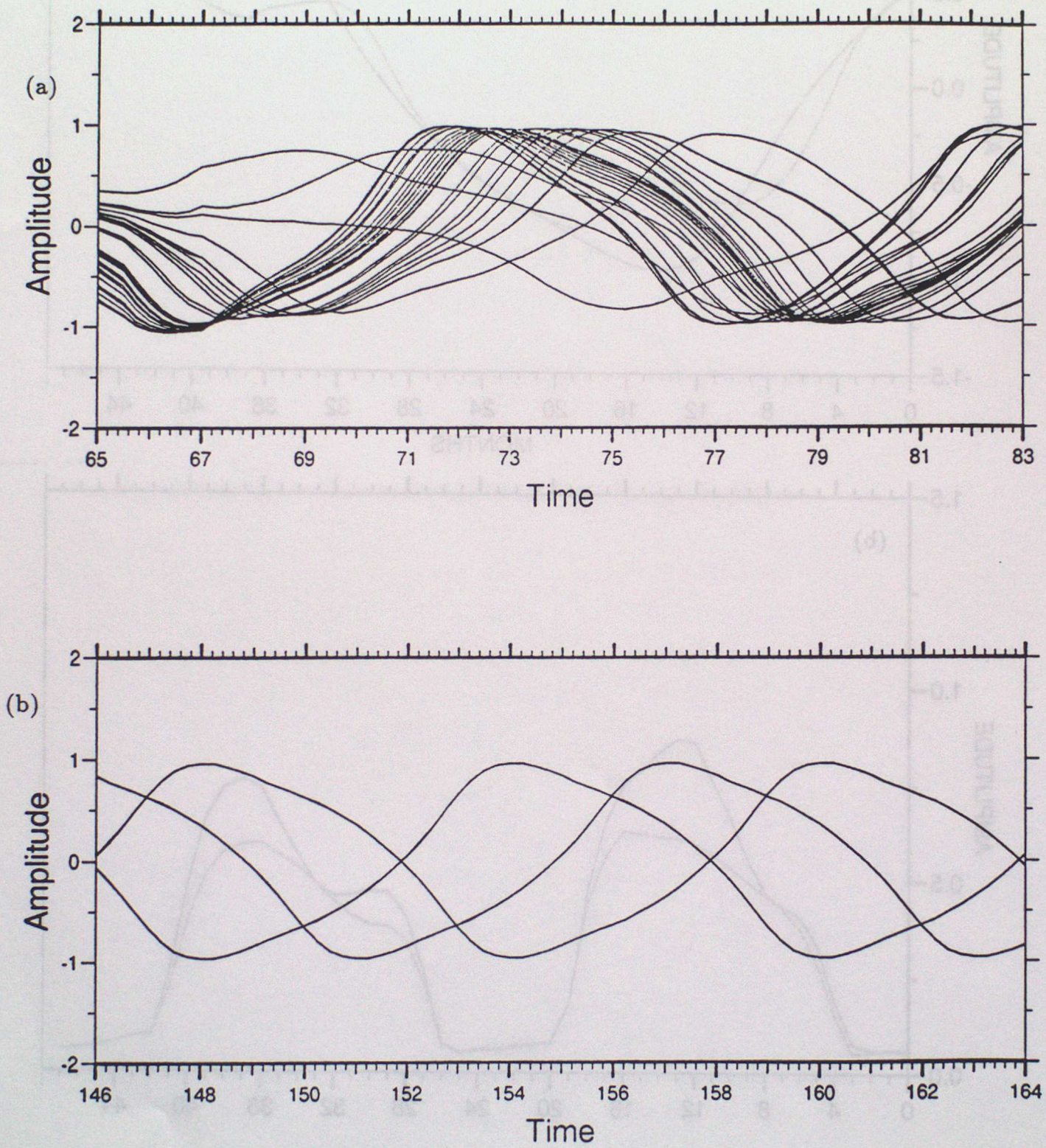

Fig. 3: Sample forecast trajectories for case I. Each forecast shown starts with the same ENSO phase and the same 'delay' values, but with different initial random perturbations. Time units are nondimensional: 1 year is equivalent to 3 units.

(a) With 3 exceptions, the forecasts tend to scatter around the same general trajectory for the first few months.

(b) After several years, the forecasts in (a) settle into 3 of the 4 possible seasonally phase-locked regular oscillations.

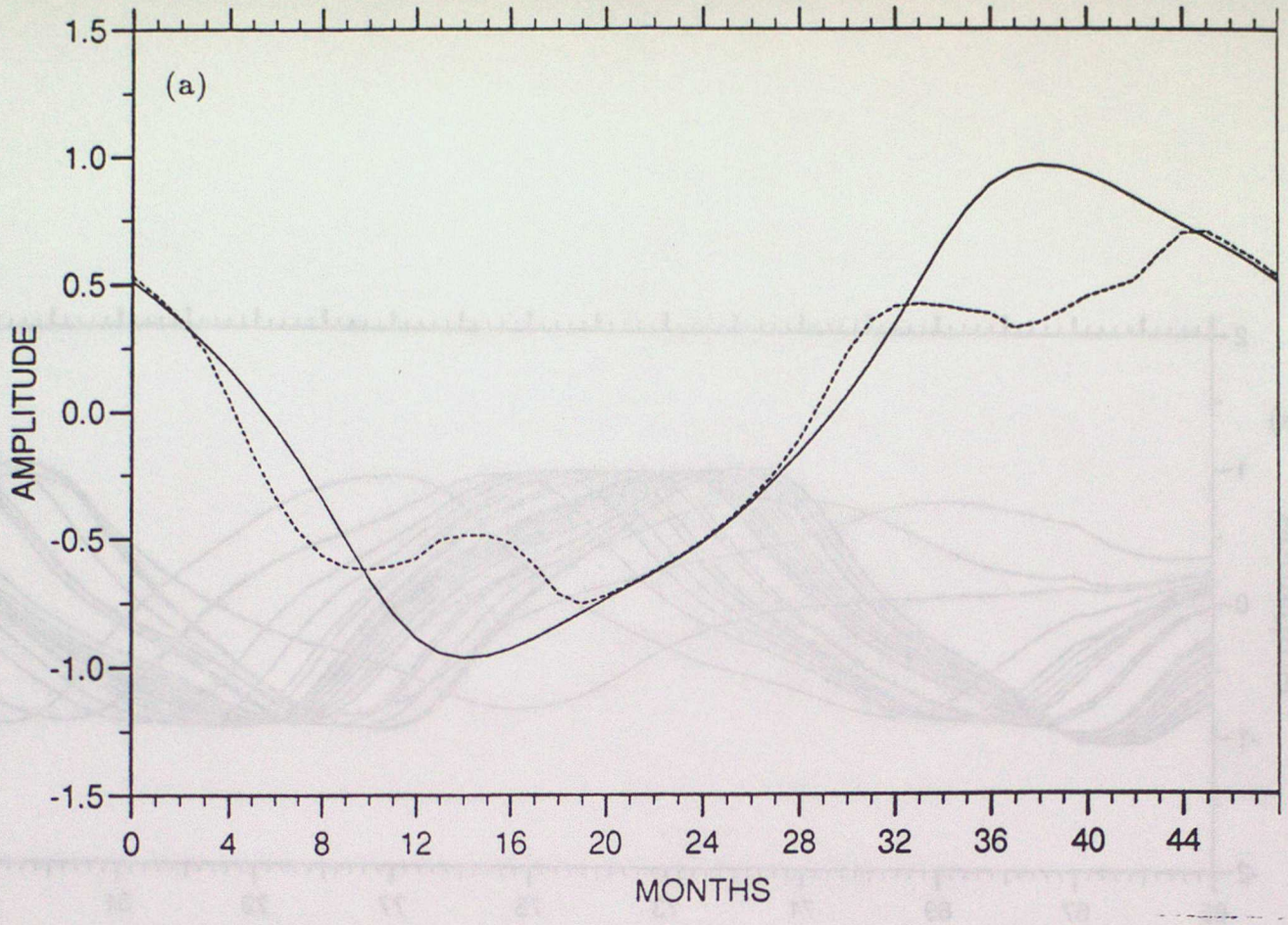

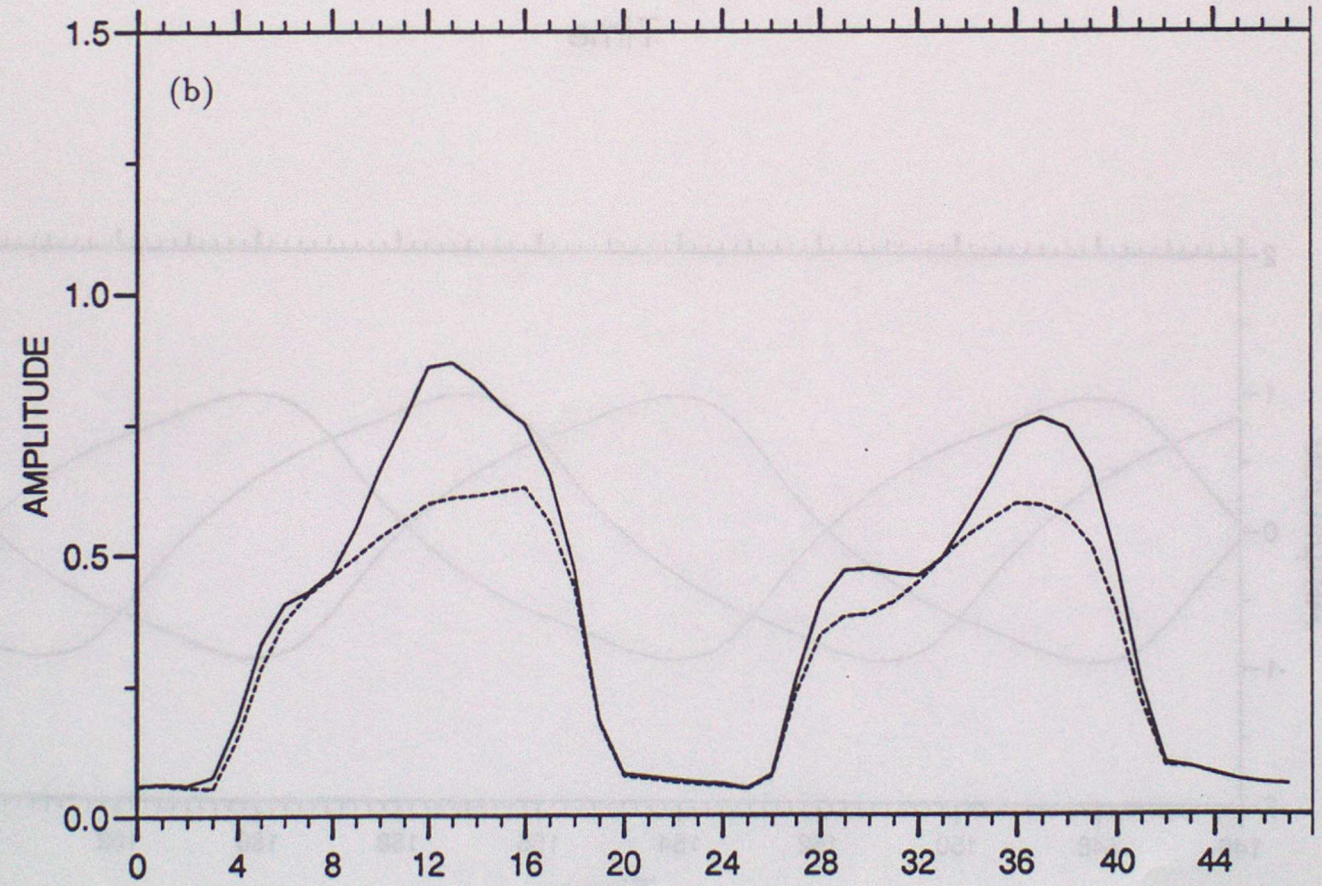

Fig. 4: Case I: values averaged with fixed ENSO phase index l

(a) The control values $\hat{C}_l$ (solid curve) correspond to a regular ENSO cycle of 48 months. The average forecast $\hat{F}_{lj}$ of $\hat{C}_l$ for a lead time of $j = 12$ months (dashed curve) is worst near peaks and troughs of $\hat{C}_l$.

(b) rms forecast error e_{lj} (solid curve) and forecast standard deviation σ_{lj} (dashed curve), averaged with fixed ENSO phase l for lead time $j = 12$ months, are similar in pattern, and largest near peaks and troughs in the control $\hat{C}_l$.

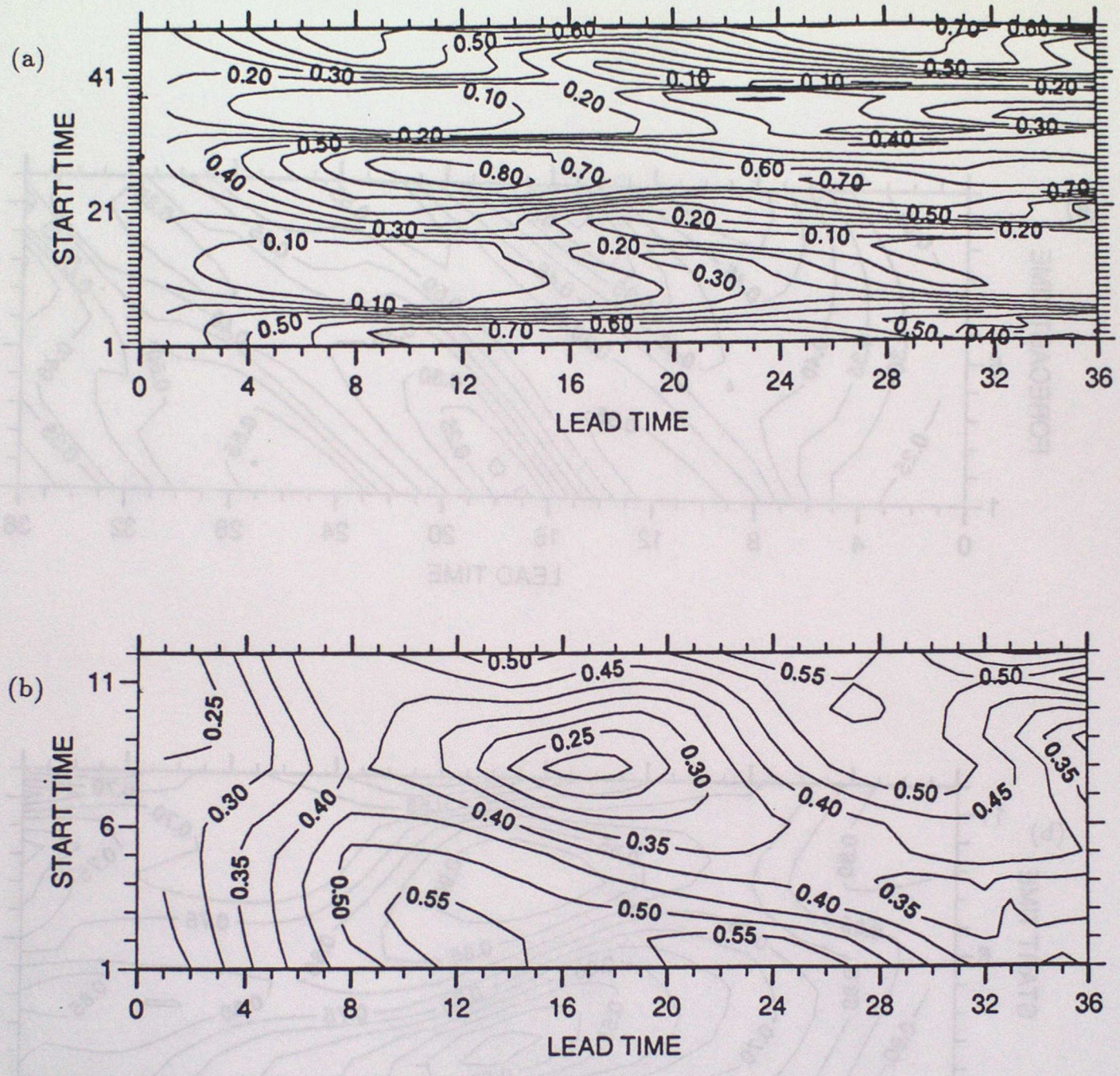

Fig. 5: Case I

(a) contours of rms forecast error e_{lj} as a function of lead time j months, and of forecast start time which is month $(l-j)$ mod 48 of the ENSO cycle.

(b) contours of rms forecast error e_{mj} as a function of lead time j months, and of forecast start time which is month $(m-j)$ mod 12 of the seasonal cycle

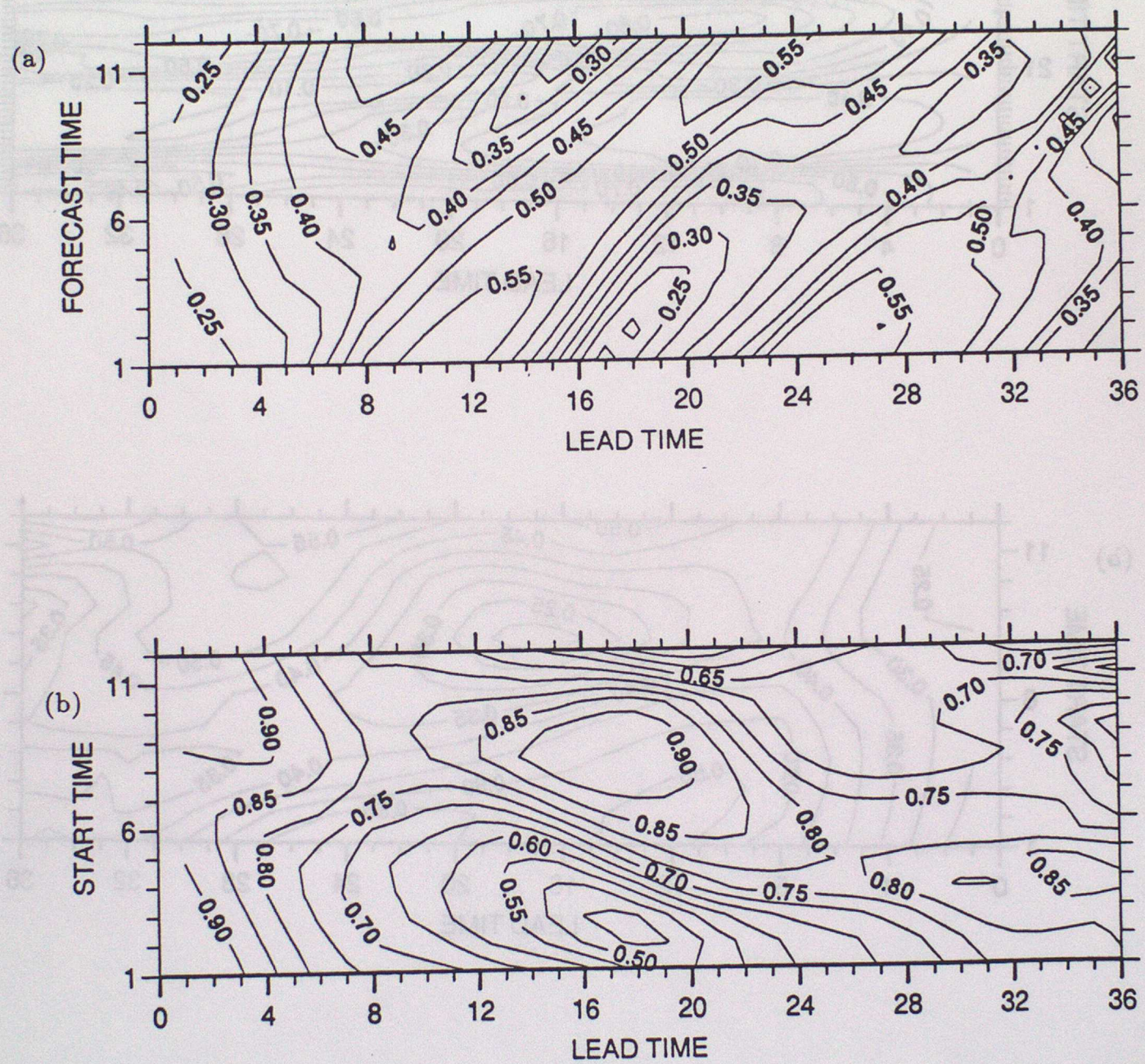

Fig. 6: Case I: values averaged with fixed month-of-year m.

(a) contours of rms forecast error e_{mj} as a function of lead time j months, and of forecast time which is month m of the seasonal cycle for which the forecast is made.

(b) contours of correlation coefficient r_{mj} as a function of lead time j months, and of forecast start time which is month $(m - j)$ mod 12 of the seasonal cycle.

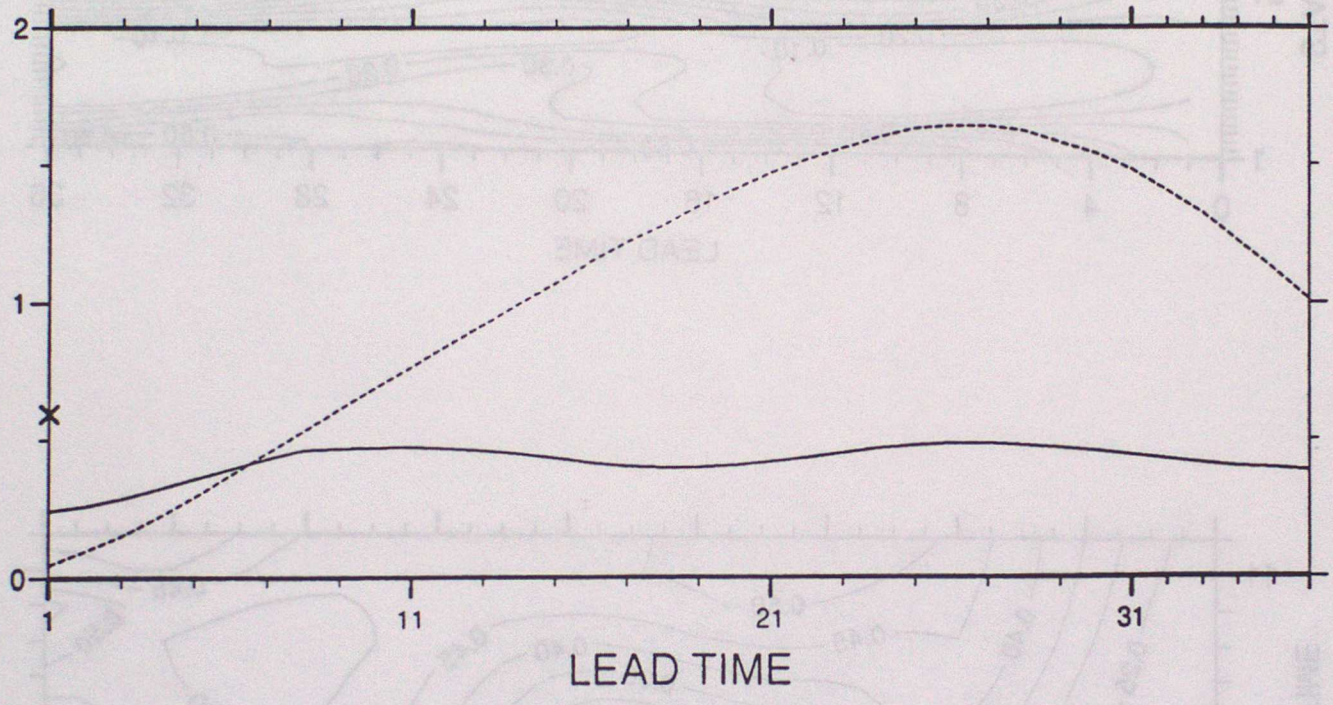

Fig. 7: Case I: values averaged over all months, to show the dependence of rms forecast error e_j (solid) and rms persistence error pe_j (dashed) on lead time j months. The marker × indicates the standard deviation σ of the control.

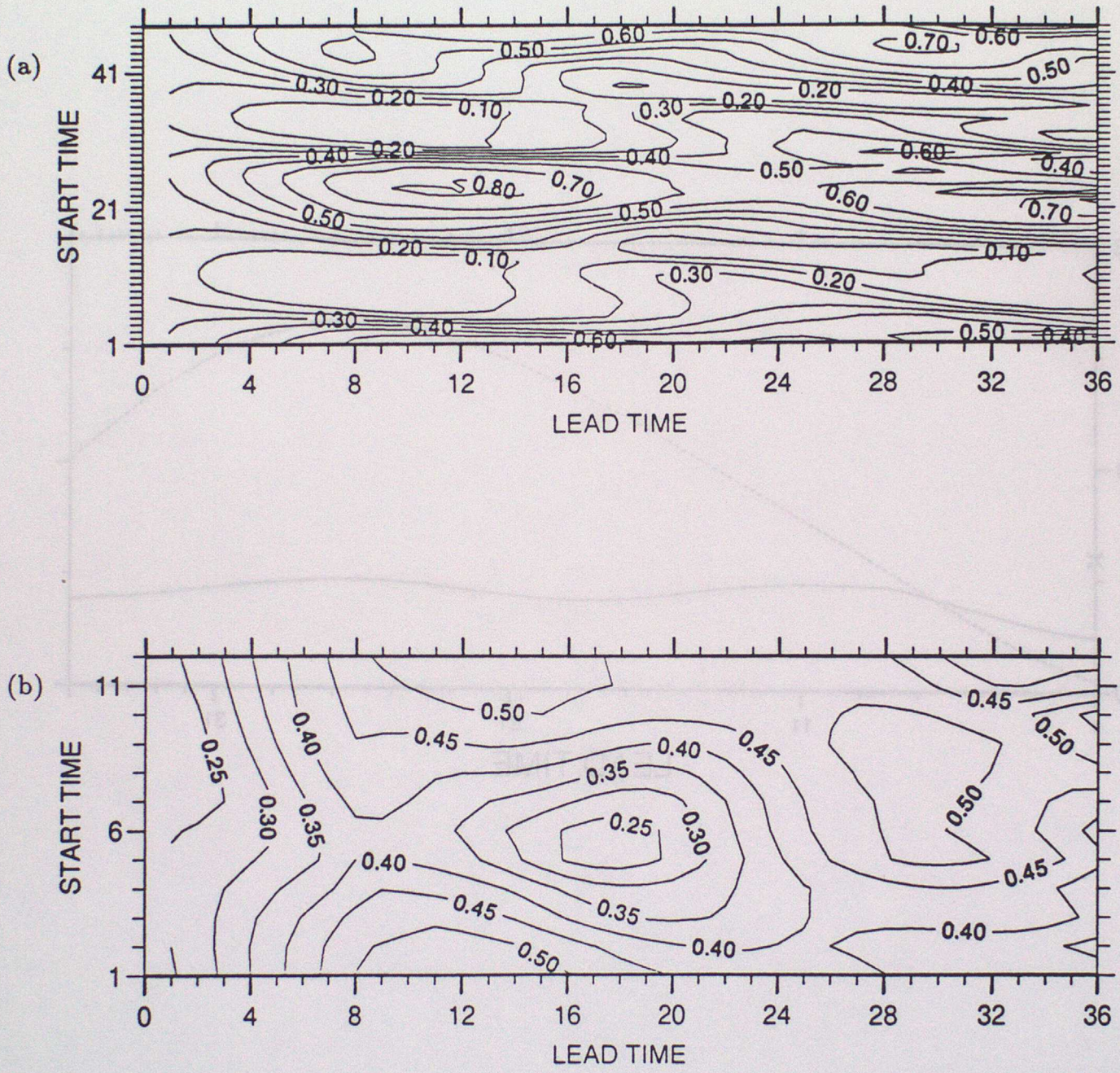

Fig. 8: Case N: no seasonal cycle of parameters α and Δ.

(a) contours of rms forecast error e_{lj} as a function of lead time j months, and of forecast start time which is month $(l-j)$ mod $12K$ of the ENSO cycle.

(b) contours of rms forecast error ϵ_{mj} as a function of lead time j months, and of forecast start time which is month $(m-j)$ mod 12 of the seasonal cycle.

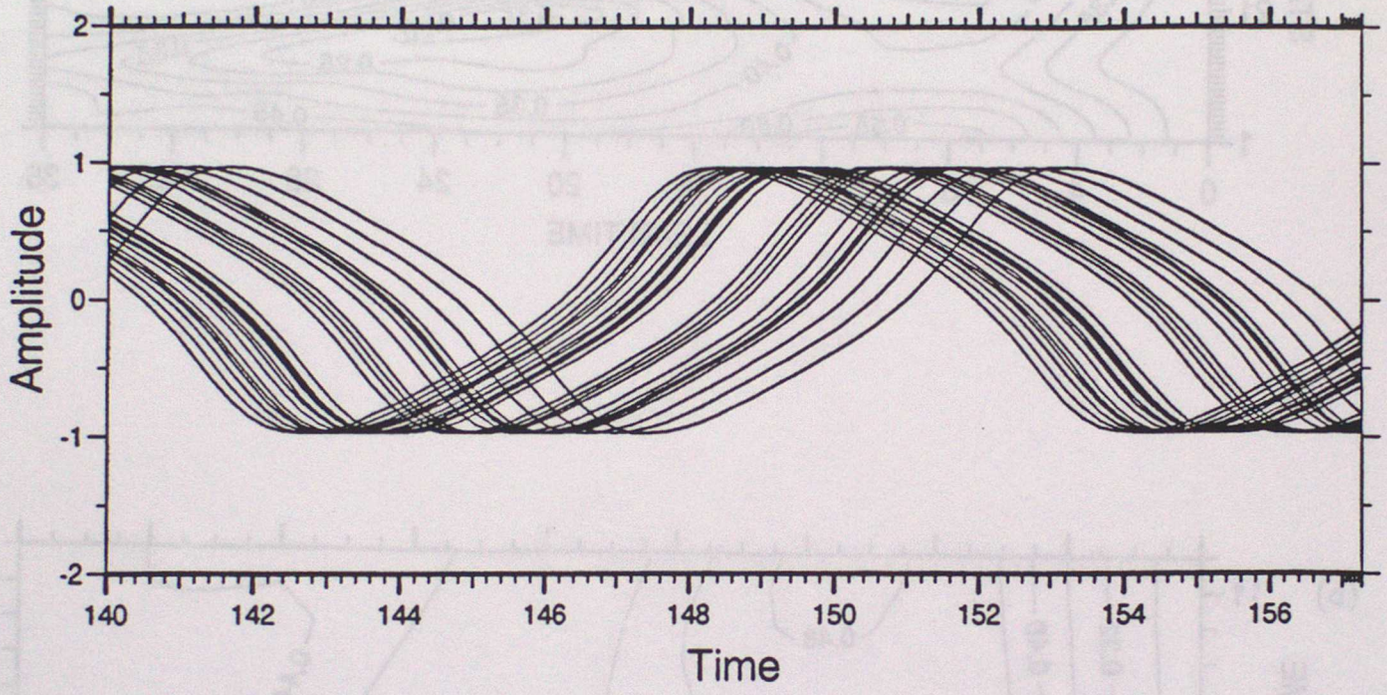

Fig. 9: Case N: no seasonal cycle of parameters α and Δ. Trajectories of sample forecasts settle into regular oscillations after several years. These oscillations are not seasonally phase-locked. Time units are nondimensional: 1 year is equivalent to 2.87 units. The regular oscillations each have a period of 4 years.

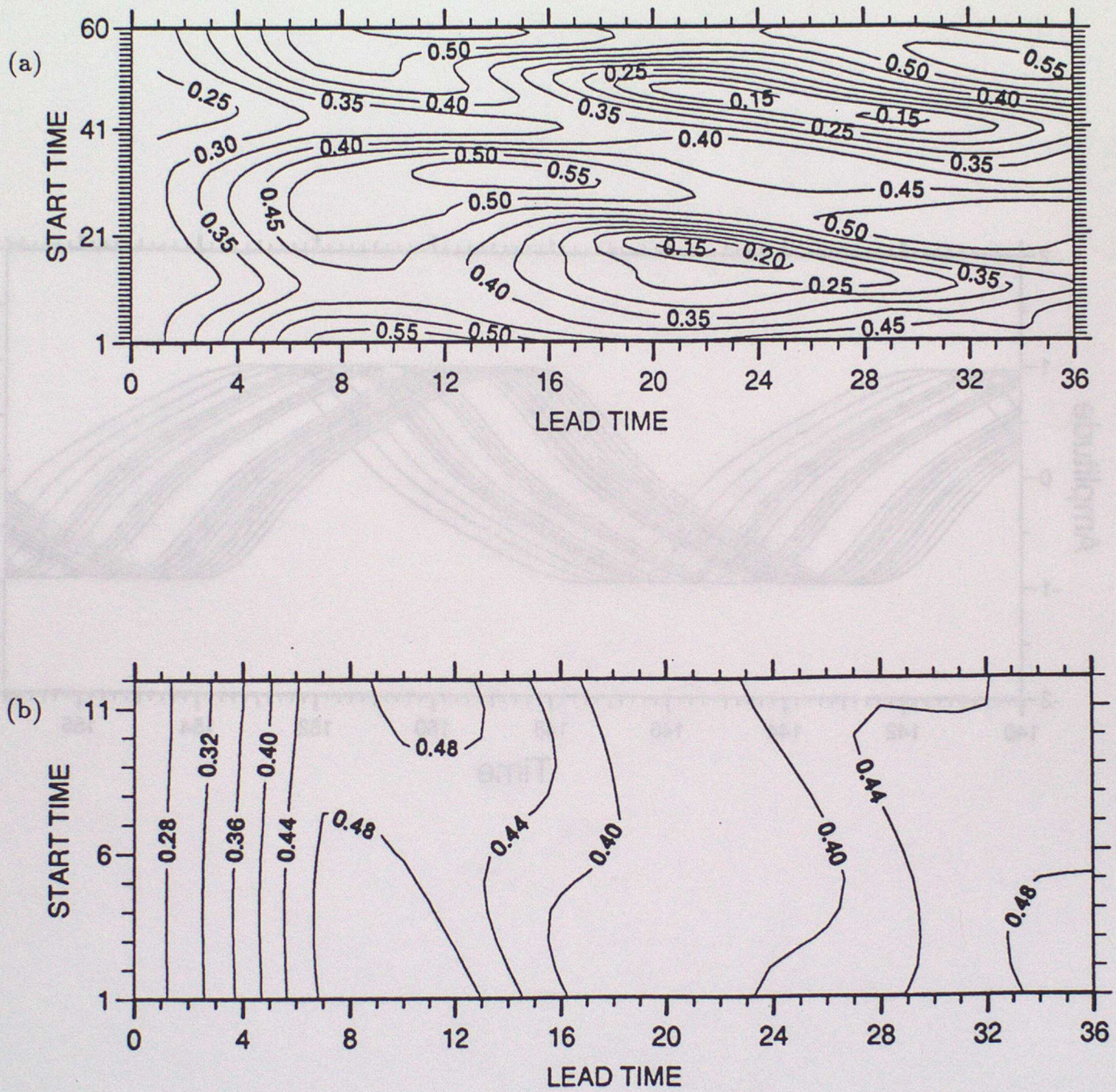

Fig. 10: Case IV:

(a) contours of rms forecast error e_{lj} as a function of lead time j months, and of forecast start time which is month $(l-j)$ mod $12K$ of the ENSO cycle.

(b) contours of rms forecast error e_{mj} as a function of lead time j months, and of forecast start time which is month $(m-j)$ mod 12 of the seasonal cycle.

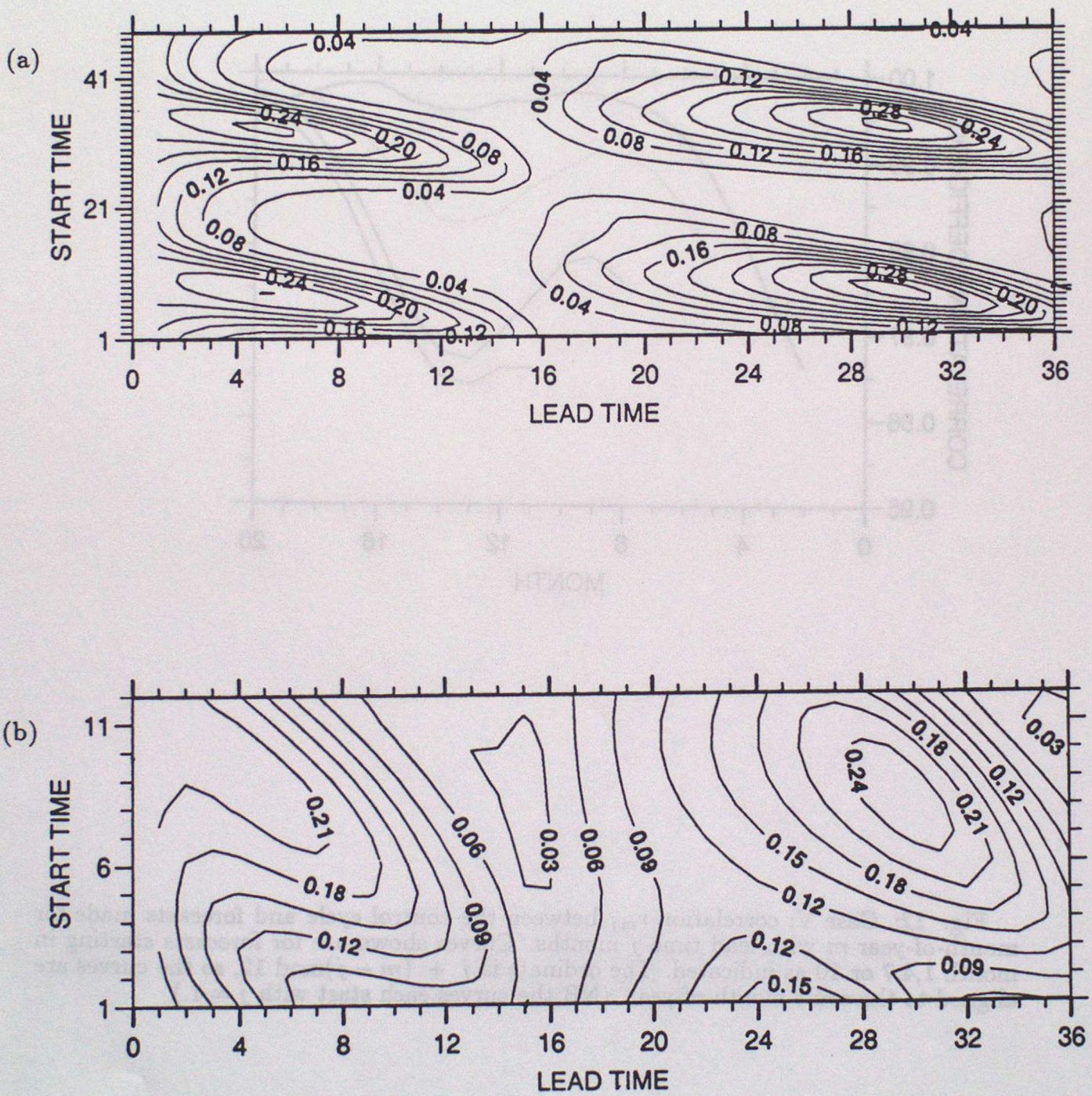

Fig. 11: Case V:

(a) contours of rms forecast error e_{lj} as a function of lead time j months, and of forecast start time which is month $(l-j)$ mod $12K$ of the ENSO cycle.

(b) contours of rms forecast error e_{mj} as a function of lead time j months, and of forecast start time which is month $(m-j)$ mod 12 of the seasonal cycle.

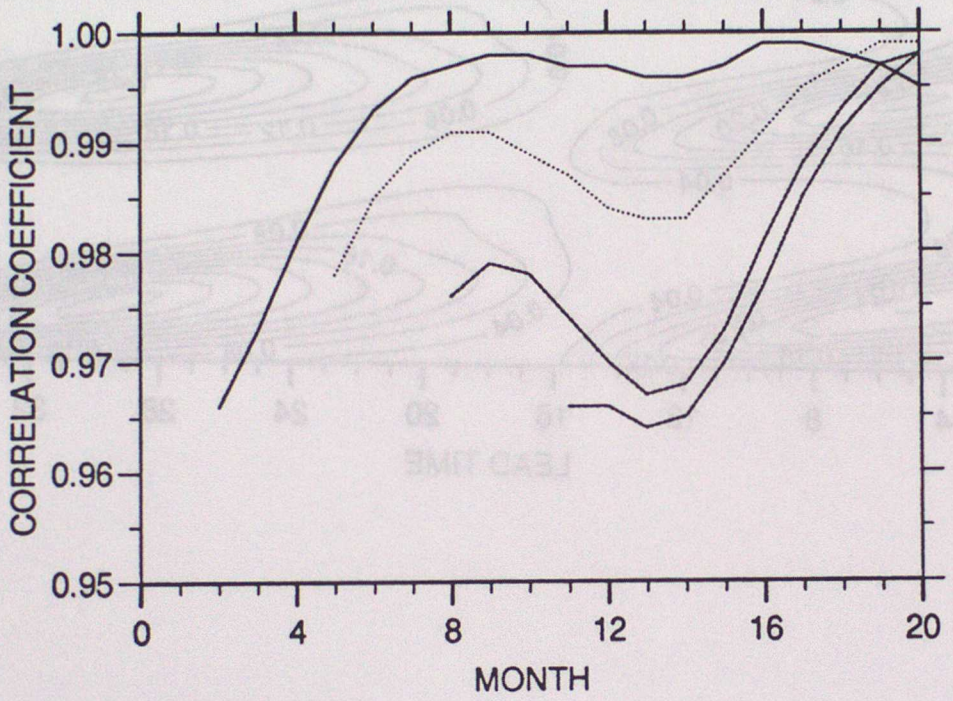

Fig. 12: Case V: correlation r_{mj} between the control cycle and forecasts made for month-of-year m with lead time j months. Curves shown are for forecasts starting in month 1,4,7 or 10 as indicated. The ordinate is $j + (m - j) \bmod 12$, so the curves are aligned to the same month-of-year. (NB the curves each start with $j = 1$.)

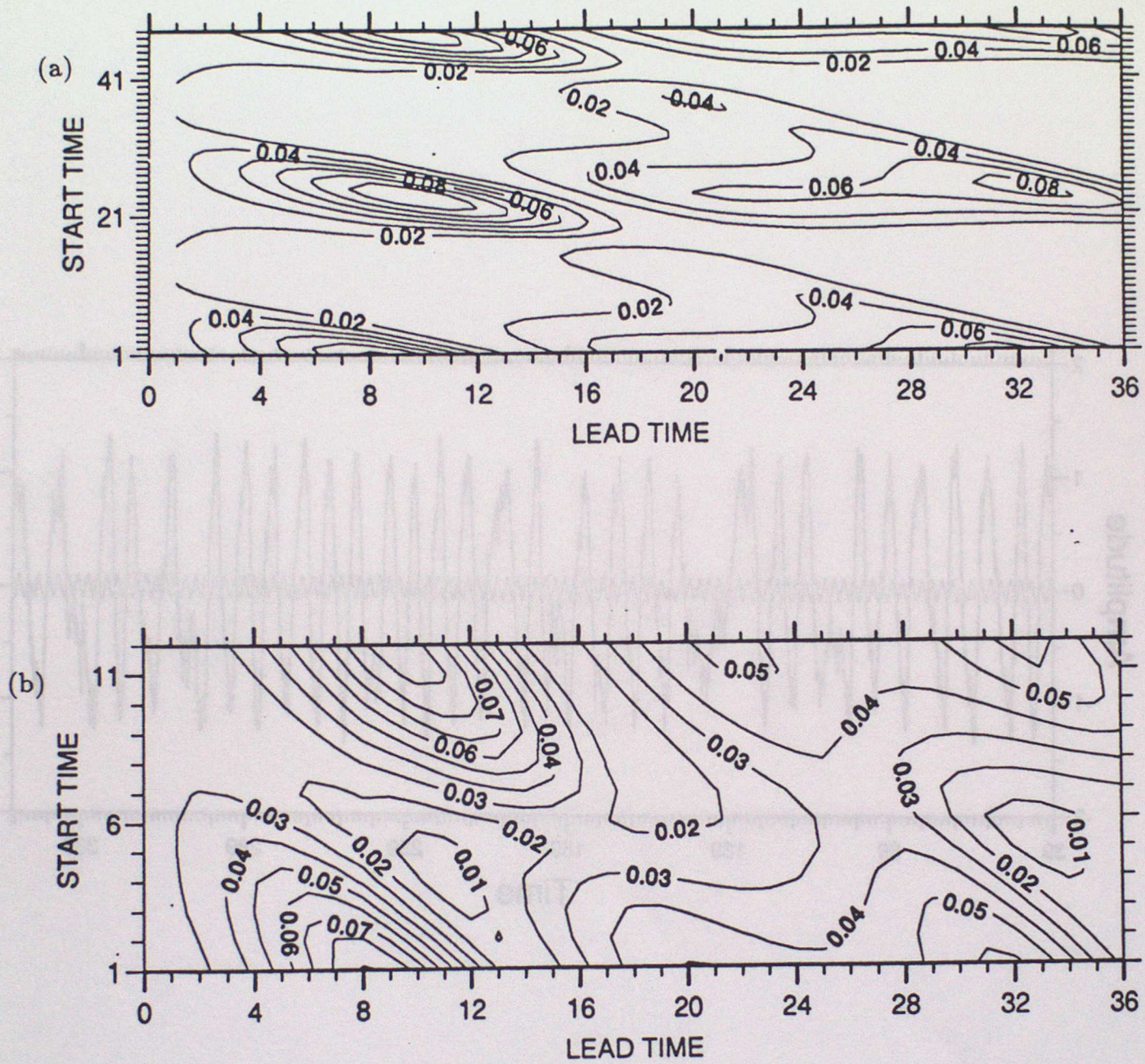

Fig. 13: Case I repeated with small initial perturbations in the range (-0.05,0.05).
(a) contours of rms forecast error e_{lj} as a function of lead time j months, and of forecast start time which is month $(l-j)$ mod 48 of the ENSO cycle.
(b) contours of rms forecast error e_{mj} as a function of lead time j months, and of forecast start time which is month $(m-j)$ mod 12 of the seasonal cycle.

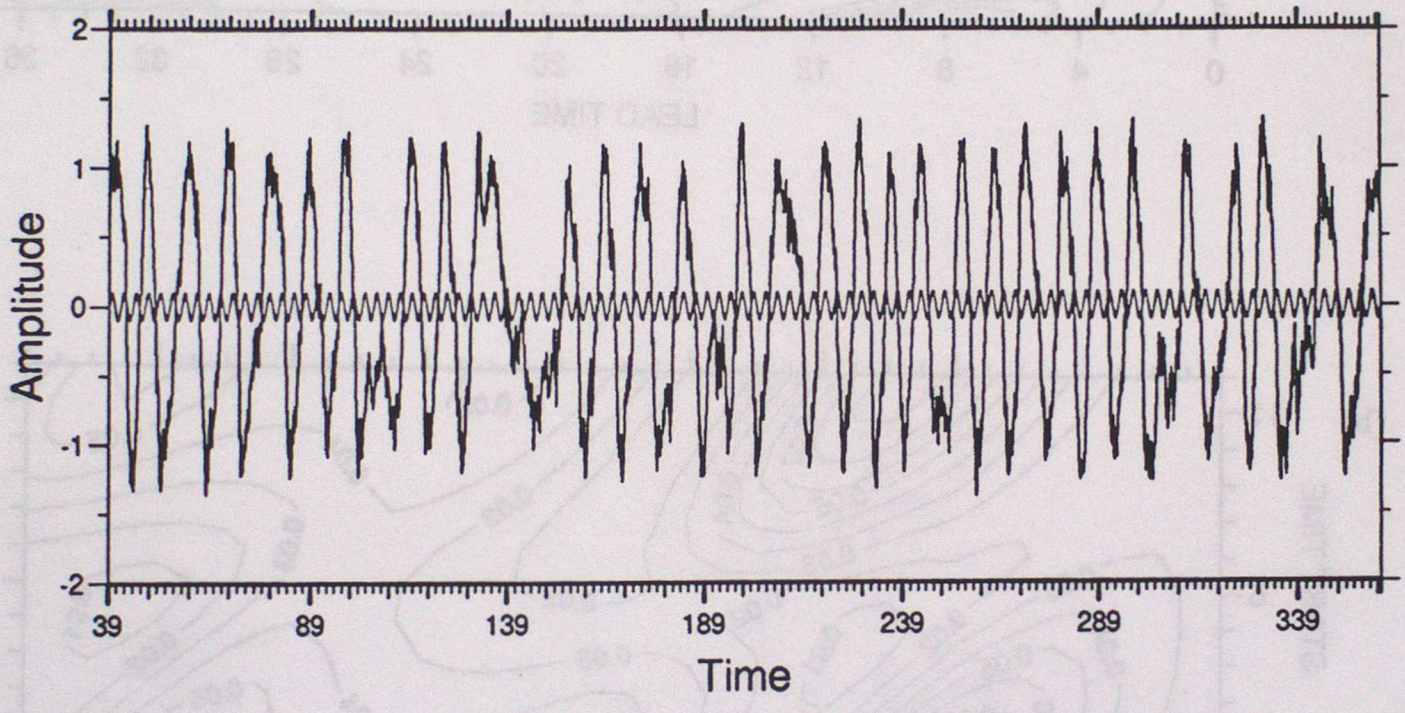

Fig. 14: Case I repeated with random noise forcing: the control C_i shown now has irregular interannual fluctuations. Time units are nondimensional: 1 year is equivalent to 3 units.

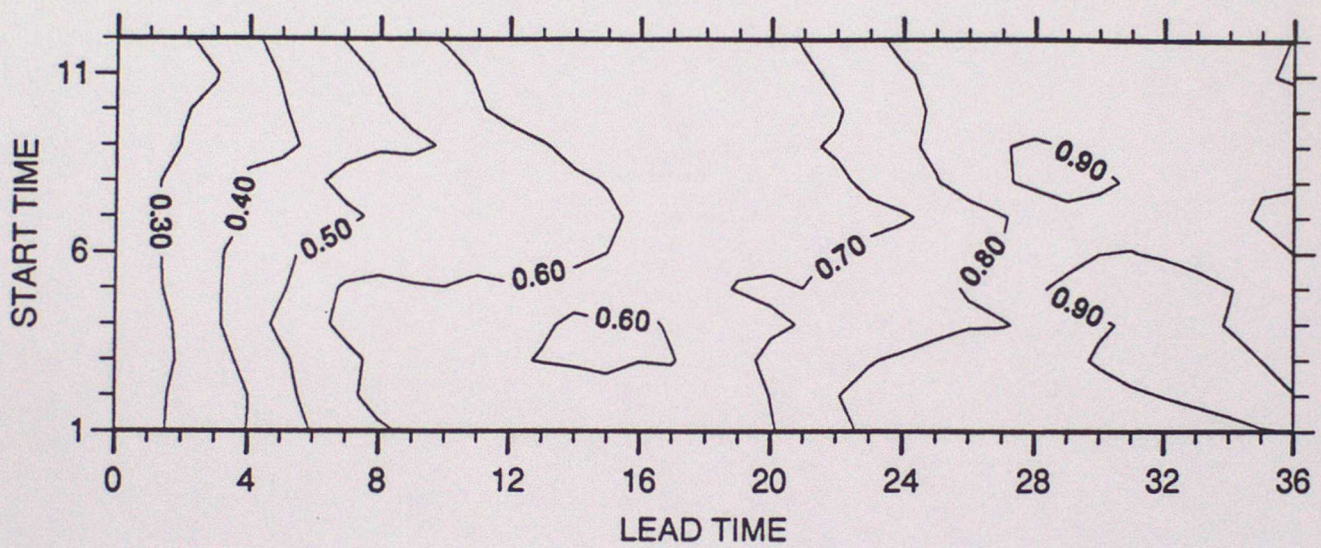

Fig. 15: Case I repeated with added random noise forcing. Contours of rms forecast error e_{mj} as a function of lead time j months and of forecast start time which is month $(m-j)$ mod 12 of the seasonal cycle. With random forcing added the ENSO cycle loses its seasonal phase locking and forecast skill has no significant seasonal dependence.

CLIMATE RESEARCH TECHNICAL NOTES

CRTN 1	Oct 1990	Estimates of the sensitivity of climate to vegetation changes using the Penman-Monteith equation. P R Rowntree
CRTN 2	Oct 1990	An ocean general circulation model of the Indian Ocean for hindcasting studies. D J Carrington
CRTN 3	Oct 1990	Simulation of the tropical diurnal cycle in a climate model. D P Rowell
CRTN 4	Oct 1990	Low frequency variability of the oceans. C K Folland, A Colman, D E Parker and A Bevan
CRTN 5	Dec 1990	A comparison of 11-level General Circulation Model Simulations with observations in the East Sahel. K Maskell
CRTN 6	Dec 1990	Climate Change Prediction. J F B Mitchell and Qing-cun Zeng
CRTN 7	Jan 1991	Deforestation of Amazonia - modelling the effects of albedo change. M F Mylne and P R Rowntree
CRTN 8	Jan 1991	The role of observations in climate prediction and research. D J Carson
CRTN 9	Mar 1991	The greenhouse effect and its likely consequences for climate change. D J Carson
CRTN 10	Apr 1991	Use of wind stresses from operational N.W.P. models to force an O.G.C.M. of the Indian Ocean. D J Carrington
CRTN 11	Jun 1991	A new daily Central England Temperature series, 1772-1991. D E Parker, T P Legg and C K Folland
CRTN 12	Jul 1991	Causes and predictability of Sahel rainfall variability. D P Rowell, C K Folland, K Maskell, J A Owen, M N Ward
CRTN 13	Jul 1991	Modelling changes in climate due to enhanced CO_2, the role of atmospheric dynamics, cloud and moisture. C A Senior, J F B Mitchell, H Le Treut and Z-X Li

CLIMATE RESEARCH TECHNICAL NOTES

CRTN 14	Sep 1991	Sea temperature bucket models used to correct historical SST data in the Meteorological Office. C K Folland
CRTN 15	Aug 1991	Modelling climate change, and some potential effects on agriculture in the U.K. P R Rowntree, B A Callander and J Cochrane
CRTN 16	Aug 1991	The Boreal Forests and Climate G Thomas and P R Rowntree
CRTN 17	Aug 1991	Development of a Stratosphere-Troposphere Data Assimilation System. R Swinbank.
CRTN 18	Sep 1991	A study of asynchronous coupling using a simple climate model. M K Davey.
CRTN 19	Sep 1991	The Oceanic Carbon Cycle. N K Taylor
CRTN 20	Nov 1991	Worldwide ocean-atmosphere surface fields in Sahel wet and dry years using provisionally corrected surface wind data. M N Ward
CRTN 21	Dec 1991	Coupled tropical ocean global atmosphere models at the UKMO. M K Davey, C Gordon, S Ineson and S Lawrence
CRTN 22	Dec 1991	Empirical parameterisation of tropical ocean-atmosphere coupling. M Allen, M K Davey, D L T Anderson and P D Killworth
CRTN 23	Feb 1992	The temporal evolution of Equatorial Currents in the Indian Ocean D L T Anderson, D J Carrington, R A Corry and C Gordon
CRTN 24	Feb 1992	Stratospheric analyses provided by the U.K. Meteorological Office M J Bailey, A O'Neill and V D Pope
CRTN 25	Feb 1992	Modelling interannual variability in the Indian Ocean using momentum fluxes from the UKMO and ECMWF operational weather analyses. D L T Anderson and D J Carrington

CLIMATE RESEARCH TECHNICAL NOTES

CRTN 26	Mar 1992	A GCM simulation of the impact of Amazonian deforestation on climate using an improved canopy representation J Lean and P R Rowntree
CRTN 27	Mar 1992	The parameterization of rainfall interception in GCMs A J Dolman and D Gregory
CRTN 28	Jun 1992	Development of worldwide marine data eigenvectors since 1985 A W Colman
CRTN 29	Jun 1992	A tropical ocean model with reduced physics M K Davey
CRTN 30	Jun 1992	International Temperature Workshop, Boulder, Colorado, USA, 16 January 1992 Edited by D E Parker
CRTN 31	Jul 1992	Simulation of clear-sky outgoing longwave radiation over the oceans using operational analyses A Slingo and M J Webb
CRTN 32	Sep 1992	A prediction of the transient response of climate J M Murphy
CRTN 33	Nov 1992	LEPS scores for assessing climate model simulations and long-range forecasts. C K Folland
CRTN 34	Jan 1993	Stratospheric Data Assimilation System Guide Editer: R Swinbank
CRTN 35	Mar 1993	A Stratosphere-Troposphere Data Assimilation System R Swinbank and A O'Neill
CRTN 36	Mar 1993	Validation of hydrological schemes for climate models against catchment data. P R Rowntree and J Lean
CRTN 37	Apr 1993	Modelling of palaeoclimates: Examples from the recent past J F B Mitchell
CRTN 38	May 1993	A simulation of seasonality in ENSO forecast skill M K Davey, D L T Anderson and S Lawrence